https://doi.org/10.1007/s41230-025-5003-3

Effect of polysilazane on microstructure and properties of Al_2O_3-based ceramic core for 3D printing

Sheng-qi Liu[1, 3], Rui-long Yu[2], Wen-jun Dong[1], *Qiao-lei Li[1], Ang Li[2], Wei Liu[2, 5, 6], Xi-he Liu[4], Xin-yan Yue[3, 7], Jing-jing Liang[1, 8], and **Jin-guo Li[1, 8]

1. Shi-changxu Innovation Center for Advanced Materials, Institute of Metal Research, Chinese Academy of Sciences, Shenyang 110016, China
2. State Key Laboratory of Advanced Casting Technologies, Shenyang 110022, China
3. Key Laboratory for Anisotropy and Texture of Materials (Ministry of Education), School of Materials Science and Engineering, Northeastern University, Shenyang 110819, China
4. China United Gas Turbine Technology Co., Ltd., Beijing 100016, China
5. School of Intelligence Science and Technology, University of Science and Technology Beijing, Beijing 100083, China
6. Beijing Advanced Innovation Center for Materials Genome Engineering, University of Science and Technology Beijing, Beijing 100083, China
7. Institute of Advanced Ceramics, School of Materials Science and Engineering, Northeastern University, Shenyang 110819, China
8. Space Manufacturing Technology (CAS Key Lab), Beijing 100094, China

Abstract: The performance of an aero-engine is closely related to the cooling ability of the hollow turbine blades. Ceramic core is an important component in the production of hollow turbine blades with a complex structure. As the pace of updating and iteration in turbine blade design continues to accelerate, the internal cavity structures of turbine blades have become increasingly complex. Traditional hot injection process is difficult to meet the production requirements of ceramic cores with complex structures. 3D printing technology can manufacture ceramic cores without the need for moulds, significantly shortening the production cycle and providing a new technology for the production of ceramic cores with complex structures. To meet the technical requirements of the investment casting process, ceramic cores must possess adequate mechanical strength and appropriate porosity. In this work, the ceramic slurry with polysilazane (PSZ) precursor was successfully prepared, and the Al_2O_3-based ceramic cores with high performance were fabricated using 3D printing technology. The regulation mechanism of polysilazane on the performance of ceramic cores was investigated. The results show that with the increase of PSZ content, the flexural strength of ceramic cores firstly increases and then decreases. When the content of PSZ is 5%, the flexural strength at 25 °C and 1,500 °C are 31.5 MPa and 13.1 MPa, respectively, and the porosity is 36.7%. This work is expected to advance the research and practical application of high-performance ceramic cores fabricated via 3D printing.

Keywords: polysilazane; ceramic core; 3D printing; flexural strength; porosity; hollow turbine blade

CLC numbers: TG221$^+$.2 **Document code:** A **Article ID:** 1672-6421(2025)05-545-10

1 Introduction

The hollow turbine blade designed with a complex internal structure provides a hollow cooling path[1]. This improves the temperature bearing capacity of turbine blades and can successfully fabricate the aero-engine with a high thrust-to-weight ratio. Ceramic cores are widely used to form complex inner cavity structures of aero-engine turbines[2], which is critical to the yield rate and quality of hollow blades[3]. Traditional processes for preparing ceramic cores are hot pressing, injection

***Qiao-lei Li**

Male, Ph. D., Assistant Researcher. His research interests mainly focus on additive manufacturing of ceramics and precision casting of single crystal blades.

E-mail: qlli@imr.ac.cn

****Jin-guo Li**

Male, Ph. D., Researcher. His research interests mainly focus on precision casting of superalloys and additive manufacturing.

E-mail: jgli@imr.ac.cn

Received: 2025-01-06; Revised: 2025-02-27; Accepted: 2025-03-18

molding, and gel casting[1, 4, 5]. However, due to the continuous updating and iteration of aero-engines, the internal structure of hollow turbine blades is becoming more and more complex, and the traditional manufacturing methods are difficult to meet the production requirements of ceramic cores with complex structures[6]. 3D printing technology has become an advanced material forming technology due to its high forming accuracy and ability to produce complex structural parts[7, 8]. Different from the traditional preparation method, 3D printing technology solidifies ceramic slurry layer by layer to form green bodies[9]. Then, the ceramic green body is degreased and sintered to obtain the product. In the above manufacturing process, the ceramic cores with complex structures can be quickly formed layer by layer without a mould[10], which provides a feasible solution for the preparation of ceramic cores with a complex structure.

Compared with silica-based ceramic cores, Al_2O_3-based ceramic cores have been widely studied and utilized due to their excellent high temperature performance and high creep resistance[11]. Generally, Al_2O_3-based ceramic cores have a higher sintering temperature, which makes them a higher flexural strength, so as to resist the impact of molten metal. However, the higher sintering temperature results in a lower porosity of the ceramic core, making it difficult to dissolve after casting[12]. Due to the contradiction between the flexural strength and porosity of Al_2O_3-based ceramic cores, how to balance the relationship between flexural strength and porosity has become a research hotspot[13-15]. Currently, the research on the porosity and flexural strength of 3D printed Al_2O_3-based ceramic cores mainly focuses on modifying the liquid phase components of the slurry[16-20], designing the material composition[21-24], and optimizing the sintering process[25, 26]. Li et al.[27] added vinyl acetate to the ceramic slurry to improve the adhesion between the alumina powder and the photosensitive resin, which effectively increased the flexural strength of the ceramic samples. Liu et al.[28] used nano-silica to improve the performance of Al_2O_3-based ceramic cores. Huo et al.[11] successfully prepared core-shell reinforced ceramic cores using SiO_2 and Y_2O_3 as mineralizers. Li et al.[29] developed a novel alumina particle grading strategy that effectively balanced the relationship between porosity and flexural strength. Li et al.[12] found that sintering temperature has a significant effect on the shrinkage and flexural strength of alumina ceramics. It can be seen from a large number of research results that the increase of sintering temperature or the addition of mineralizers can effectively improve the mechanical properties of ceramic cores, but the decrease of porosity will seriously affect the leaching efficiency of the ceramic cores.

Ceramic slurry is the prerequisite for the production of high performance ceramic cores. However, most of studies on ceramic slurry have mainly focused on improving solid loading capacity and curing properties[30, 31], with limited research addressing the fundamental design of slurry composition. In recent years, the addition of polymer precursors to ceramic slurry and then directly transforming them into ceramics through pyrolysis has become a new strategy for the preparation of ceramic materials[32, 33]. The low pyrolysis temperature of ceramic polymer precursor significantly reduces the sintering temperature[34]. In addition, the polymer precursors used in ceramic materials mainly include polyborsilane, polysiloxane, and polysilazane, and the silicon carbonitride synthesized by the pyrolysis of these precursors can improve the high-temperature performance of ceramic cores[35]. Hu et al.[36] combined polysilazane and alumina powder to prepare a ceramic precursor, which was successfully transformed into the core-shell silicon oxycarbide ceramic part with excellent properties via pyrolysis at different temperatures. Xiao et al.[37] prepared a type of photocurable preceramic resin containing silica particles, and successfully prepared ceramic green bodies using digital light processing technology. After pyrolysis, high-performance ceramic composite materials with enhanced mechanical properties were obtained.

In this work, alumina ceramic slurry with polysilazane precursor was prepared, and Al_2O_3-based ceramic core was successfully prepared using 3D printing technology. The influence of polysilazane content on the properties of ceramic slurry and the resulting ceramic core was investigated, and the underlying regulation mechanism of polysilazane on the properties of ceramic core was analyzed.

2 Experimental procedure

2.1 Raw materials

The ceramic powders used to prepare the ceramic slurry were alumina with a purity of 99.55wt.% (Hecheng New Material Co., Ltd., China). The particle size of the matrix powder was measured using a laser particle size analyzer (LA-920, Japan). Figure 1 shows the particle size distribution of the powder, which exhibits a trimodal distribution. The particle sizes corresponding to each peak are 0.67 μm, 7.01 μm, and 29.77 μm, respectively. The median diameter is 14.46 μm. The liquid phase of the slurry contained photosensitive resin [DSM (China) Co., Ltd.], dispersant (EFKA FA 4608, BASF, The Netherlands), and polysilazane (99% purity, Anhui Ayotta Silicon Oil Co., Ltd.). Photopolymerization was initiated by photoinitiator 819. The addition of polysilazane was 3%, 5%, 8%, and 10%, respectively.

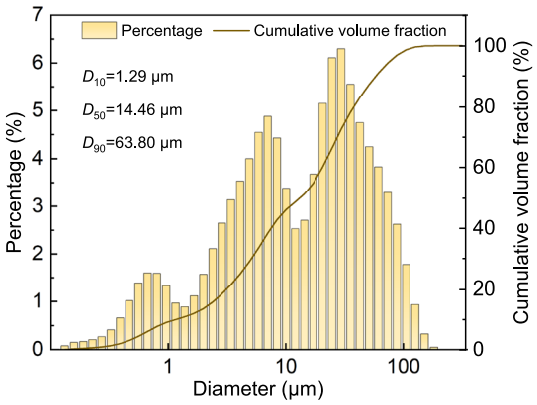

Fig. 1: Particle size distribution of alumina powder

2.2 Ceramic core preparation

Figure 2 shows the preparation diagram of an Al_2O_3-based ceramic core with polysilazane addition. Firstly, the liquid phase was prepared by mixing a photosensitive resin, polysilazane, and a dispersant in a resin-to-dispersant mass ratio of 7:3. The alumina powder was then mixed with the liquid phase and the ceramic slurry was prepared by stirring with a mixer. After that, the ceramic slurry was put into the grinding tank and then, zirconia grinding balls were added. Finally, the ceramic slurry with a solid load of 45vol.% was obtained by grinding with a planetary ball mill (Changsha Mickey Instruments Co., Ltd., China) for 2 h. After vacuum defoaming, the Al_2O_3-based ceramic green body was prepared using the 3D printing equipment (Beijing Shiwei Technology Co., Ltd., China).

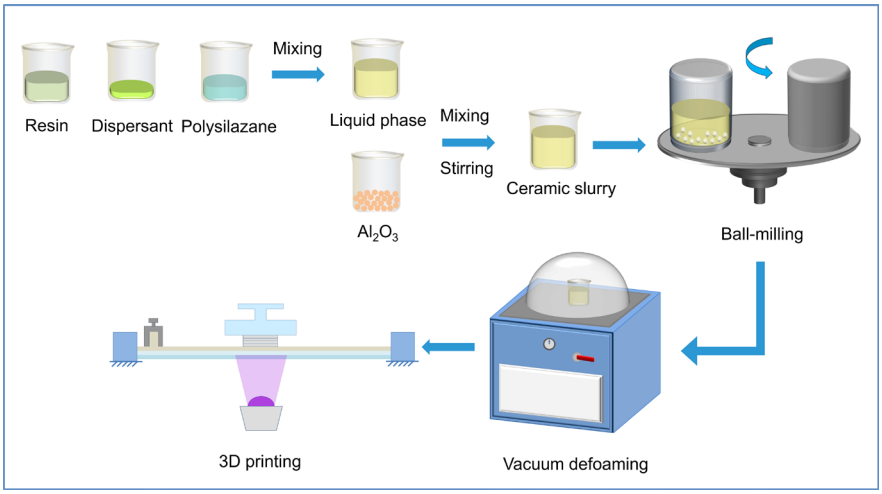

Fig. 2: Schematic showing the fabrication of Al_2O_3-based ceramic samples with polysilazane addition

The 3D printing equipment diagram is shown in Fig. 3. During the printing process, a layer of ceramic slurry was spread by a scraper. Then, the printing platform descended to the slurry layer. The ceramic slurry was irradiated and the first layer was cured to the printing platform. The layer thickness was equal to slice thickness. After the curing process was completed, the printing platform rose a certain distance, and the scraper spread a layer of slurry again. Repeat these steps until the ceramic green body was printed. The ceramic green bodies were degreased and sintered in a muffle furnace (Shanghai Quanshuo Electric Furnace Co., Ltd.). Firstly, the ceramic green body was heated to 500 °C at a rate of 2 °C·min^{-1} and held for 750 min. Then, heated to 1,000 °C at a rate of 1 °C·min^{-1} and held for 1,000 min. Finally, the ceramic green body was heated to 1,450 °C at a rate of 0.5 °C·min^{-1} and held for 400 min. After sintering, the ceramic green body was cooled in the muffle furnace.

2.3 Microstructure and properties

The microstructure of the sintered samples was observed by means of field emission scanning electron microscopy and energy dispersive spectrometry (FE-SEM; Quanta FEG 250, FEI Co. Ltd., USA). The morphology and elemental distribution of the ceramic core were characterized by transmission electron microscopy (TEM; Themis Z, FEI, USA).

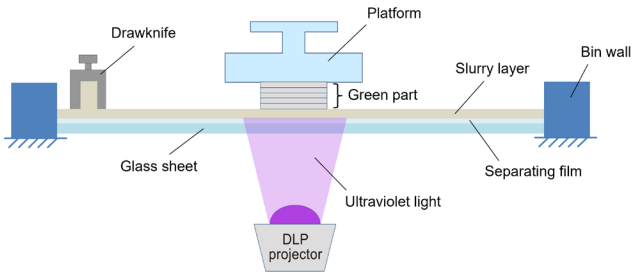

Fig. 3: Schematic diagram of 3D printing equipment

After degreasing and sintering, the volume of the ceramic samples has a certain degree of shrinkage. The size of the ceramic samples was measured using a vernier caliper. The sintering shrinkage (δ) was calculated according to the dimensional variation of the samples in three directions. The sintering shrinkage was calculated by:

$$\delta = \frac{L - L_1}{L} \times 100\% \quad (1)$$

where L is the size of the ceramic sample before sintering, and L_1 is the size of the ceramic sample after sintering.

The porosity of the ceramic samples was measured by Archimedes drainage method. The porosity (P) of the ceramic samples was calculated by Eq. (2):

$$P = \frac{m_3 - m_1}{m_3 - m_2} \times 100\% \quad (2)$$

where m_1 is the dry weight of the ceramic sample, m_2 is the floating weight, and m_3 is the wet weight.

The flexural strength of the samples was tested at room temperature (25 °C) and high temperature (1,500 °C). During the high-temperature strength test, the heating rate was 8 °C·min^{-1} and the holding time was 15 min. The flexural strength (σ) of the ceramic samples was measured by the three-point flexural test and calculated using the following equation:

$$\sigma = \frac{3Fs}{2bh^2} \quad (3)$$

where F is the load on the specimen, s is the distance between

the two fulcrums, and b and h are the width and thickness of the specimen, respectively.

3 Optimization of printing parameters

In order to optimize the printing parameters and ensure the successful printing of the ceramic cores, the effects of different contents of polysilazane on the curing depth of slurries were studied. Exposure time and exposure power are important parameters that affect curing depth. The relationship between curing depth and actual exposure power can be characterized by the Beer-Lambert law[38, 39], as shown in Eq. (4):

$$C_p = D_p \ln(E/E_c) \quad (4)$$

where C_p is the curing depth of the ceramic slurry after ultraviolet irradiation, D_p is the depth of ultraviolet penetration, E_c is the critical exposure energy, and E is the actual exposure energy during printing.

Figures 4(a) to (d) show the curing depth of ceramic slurry with different polysilazane contents at different exposure power and exposure time. For ceramic slurry with different polysilazane contents, the curing depth increases gradually with the increase of both exposure power and exposure time. In the 3D printing process, the greater the curing depth, the greater the bond strength between the adjacent layers of the ceramic green body, which is beneficial to resist crack propagation and improve mechanical properties. The curing depth is generally 1.5 to 2 times the layer thickness to ensure printing of qualified ceramic green bodies[22]. In this study, the layer thickness of the printer was set to 100 μm. As shown in Fig. 4, both 5 s and 6 s are within the acceptable range; considering the team's previous research results, 6 s was ultimately selected. Thus, the optimal printing parameters of the 3D printing ceramic slurry with polysilazane addition are determined to be an exposure power of 6 mW·cm^{-2} and an exposure time of 6 s. Under these conditions, the curing depth of ceramic slurry with different polysilazane contents are within a reasonable range.

4 Results and discussion

4.1 Microstructure and phase constitution

Figures 5(a) to (d) shows the room-temperature fracture morphology of ceramic cores containing different polysilazane contents, fabricated under optimal printing parameters: an exposure power of 6 mW·cm^{-2} and an exposure time of 6 s. In Fig. 5, large alumina particles are represented by yellow dotted lines, intergranular fractures are represented by green dotted lines, and transgranular fractures are represented by red dotted lines. Pores are observed in all the ceramic samples with different polysilazane contents, which are attributed to the removal of resin at high temperatures. The existence of pores is conducive to the leaching of ceramic cores. Figure 5(a) shows an SEM image of the fracture surface of the ceramic sample with a polysilazane content of 3%. Alumina particles with a smooth surface can be clearly observed, indicating that the fracture mode is intergranular fracture. The bonding strength between the ceramic particles is weak. When the addition of polysilazane increases to 5%, the fracture mode of the ceramic core is a mixed fracture mode, in which intergranular fracture and transgranular fracture exist simultaneously, as shown in

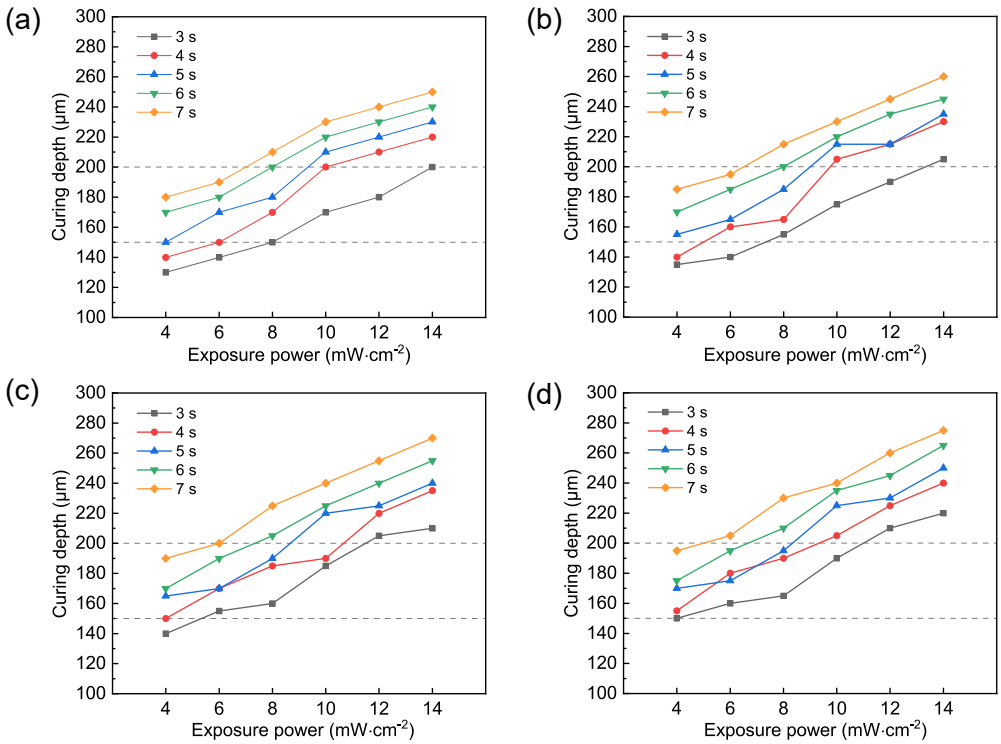

Fig. 4: Curing depth of ceramic slurry with different polysilazane contents: (a) 3%; (b) 5%; (c) 8%; (d) 10%

Fig. 5(b). As shown in Fig. 5(c), when the content of polysilazane is 8%, the fracture mode is still a mixture of transgranular and intergranular fracture, but predominantly transgranular fracture. While, as the content of polysilazane exceeds 8%, the bonding strength between the particles increases and the fracture mode is transgranular fracture. The strengthening mechanism of polysilazane on the flexural strength of the ceramic cores will be discussed in the following section.

To further analyze the pyrolysis of polysilazane and the strengthening mechanism of Al_2O_3-based ceramic cores, the elemental distribution of ceramic cores with different polysilazane contents was characterized, as shown in Fig. 6. As the matrix powder of the ceramic cores is alumina, both the Al and O elements are distributed throughout the ceramic cores, regardless of polysilazane content. In addition to Al and O, enriched Si, C, and N can also be observed, and there are

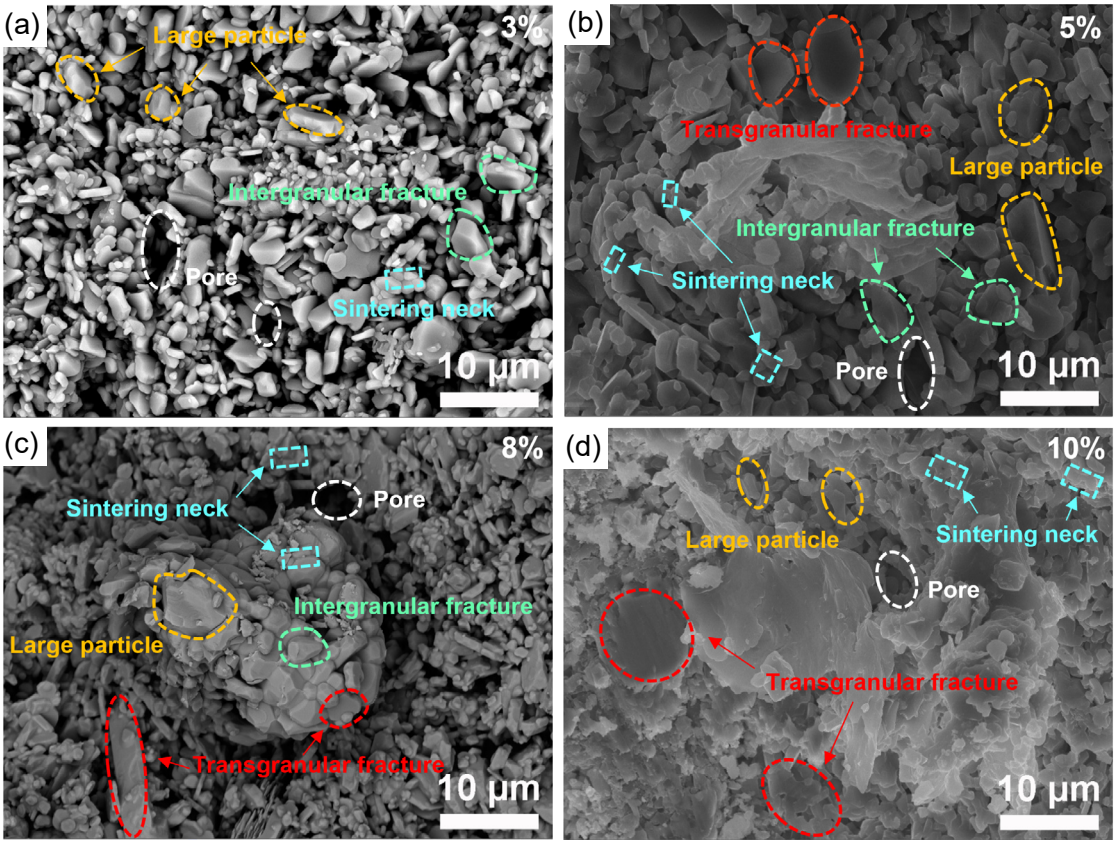

Fig. 5: SEM images of sintered ceramic samples with different polysilazane contents: (a) 3%; (b) 5%; (c) 8%; (d) 10%

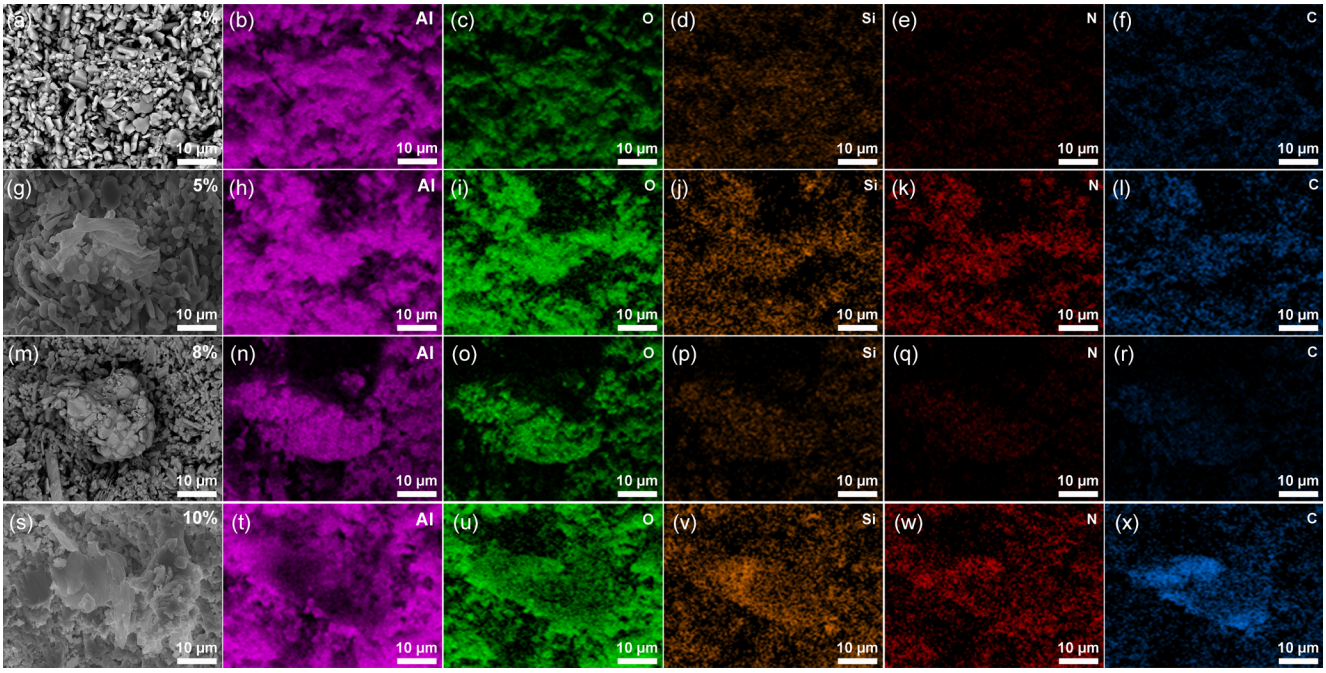

Fig. 6: Elemental distribution of ceramic samples with different polysilazane contents: (a–f) 3%; (g–l) 5%; (m–r) 8%; (s–x) 10%

overlapping areas of enrichment of these three elements. With the increase of polysilazane content, the concentration of Si, N, and C in the aggregation area increases, which indicates that SiCN is formed during the pyrolysis of polysilazane.

Figure 7 shows the XRD patterns of the ceramic cores with different contents of polysilazane. Since the matrix of the ceramic core is alumina, the XRD of the ceramic cores with different contents of polysilazane contains alumina diffraction peaks (PDF#46-1212). When the content of polysilazane is 3%, the diffraction peak of silica (PDF#74-0764) can be observed. With the increase of the content of polysilazane, the intensity of the diffraction peak of silica increases slightly, which indicates that the decomposition product of polysilazane is silica. According to previous study[40], polysilazane can be pyrolyzed into SiCN and SiO_2 after pyrolysis at high temperatures. When the sintering temperature is 1,450 °C, SiO_2 produced by the pyrolysis of polysilazane reacts with Al_2O_3 to form mullite. Therefore, when the content of polysilazane is 10%, the diffraction peak of mullite (PDF#79-1458) can be observed in the XRD pattern. While, as the content of polysilazane is less than 10%, there is no significant diffraction peak of mullite, which may be due to the low content of mullite. Another decomposition product of polysilazane is SiCN. Because SiCN is amorphous, there is no obvious diffraction peak in the XRD pattern[36, 40]. However, the distribution of elements in Fig. 6 can prove the existence of SiCN.

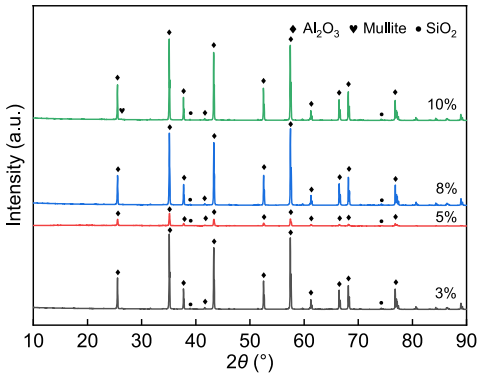

Fig. 7: XRD patterns of sintered ceramic samples with different polysilazane contents

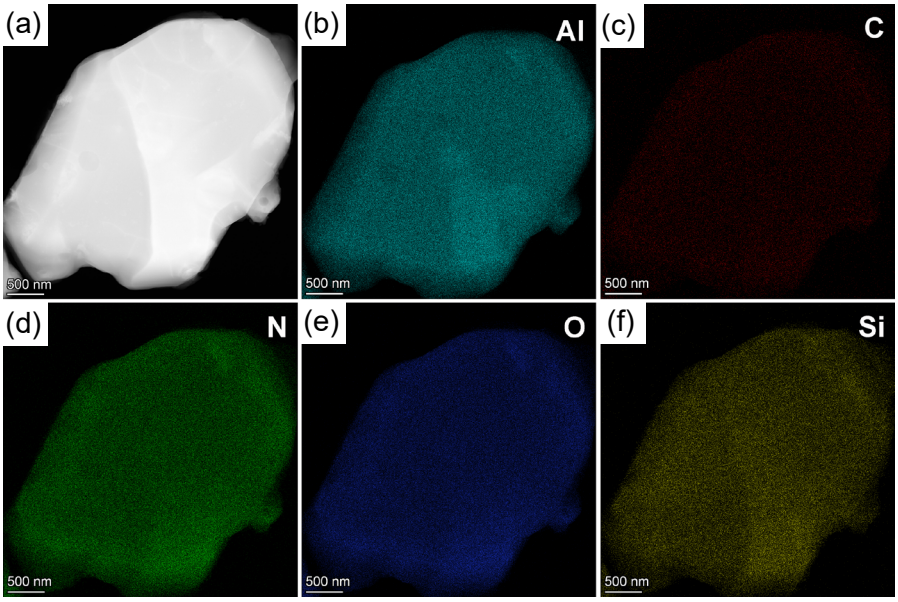

Fig. 8: TEM images of a sintered ceramic sample with 5% polysilazane content: (a) TEM analysis result; (b–f) elemental distribution

To explore the influence mechanism of polysilazane decomposition products on the properties of ceramic cores, the element distribution of ceramic particles was analyzed by TEM, as shown in Fig. 8. Consistent with the above analysis results, Al, O, C, N, and Si elements are detected on the particle surface. This proves that the pyrolysis products of the polysilazane adhered to the surface of the matrix particles. The Al-, O-, and Si-enriched regions on the particle surface are found to overlap, as shown in Figs. 8(b), (e), and (f). This may be due to that the SiO_2 generated during the pyrolysis of polysilazane reacts with Al_2O_3 to form mullite.

4.2 Shrinkage and open porosity of ceramic cores

Figure 9 shows the shrinkage and open porosity of sintered ceramic cores with different polysilazane additions. Figure 9(a) shows the shrinkage of the ceramic core in different directions. With the increase of polysilazane content, the shrinkage of the core in the *X* (length) and *Y* (width) directions firstly decreases and then increases, and slightly decreases again when the polysilazane content reaches 10%, while the shrinkage in the *Z* (height) direction decreases gradually. During the heat treatment process, the green body of the ceramic core generally goes through two stages: low-temperature degreasing and high-temperature sintering. Firstly, the resin in the ceramic green body is removed at a low temperature, leaving a large number of pores. Then, the ceramic particles are combined and grown at high temperatures, thus, the porosity and volume of the ceramic core decrease. The pyrolysis of polysilazane takes place mainly in the second stage of the heat treatment

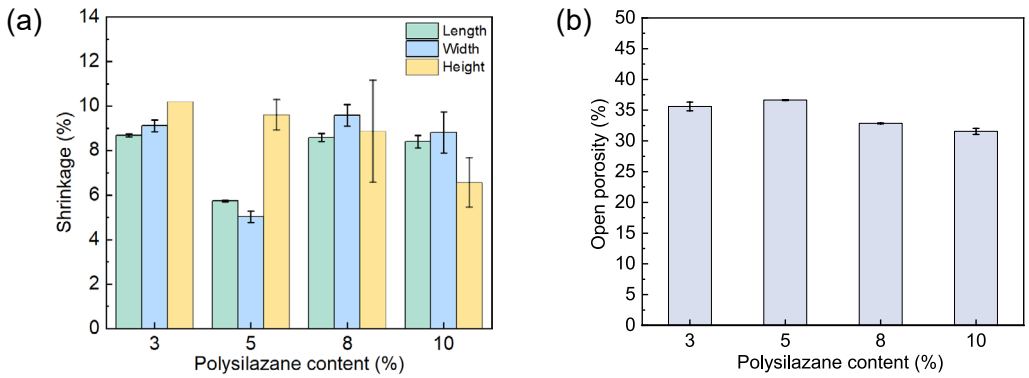

Fig. 9: Effect of polysilazane content on shrinkage (a) and open porosity (b) of ceramic samples

process, and a large number of small particles are produced from the decomposition of polysilazane. When the content of polysilazane is less than 5%, the driving force of sintering mainly comes from the matrix particles. The large particles in the ceramic core form the framework, while the small particles produced by the pyrolysis of polysilazane fill the pores, reducing sintering shrinkage by suppressing the approach of large particles during the sintering process. At this time, the sintering shrinkage of the ceramic cores gradually decreases. When the content of polysilazane exceeds 5%, a great number of small particles produced by the pyrolysis of polysilazane increase the surface energy of the system, enhance the sintering driving force, and promote sintering shrinkage along *X* and *Y* directions. Therefore, the shrinkage of the ceramic cores gradually increases. However, the small particles aggregated between the layers can effectively fill the interlayer gap, compensate for the volume shrinkage, and reduce the sintering shrinkage in the *Z* direction. Figure 9(b) shows the changing trend of porosity of ceramic cores with polysilazane content. Contrary to the trend of sintering shrinkage, the porosity of the ceramic cores increases slightly and then decreases continuously with the increase of polysilazane content. When the content of polysilazane is 5%, the porosity of the core reaches a maximum of 36.7%. A larger porosity can improve the leaching performance of the ceramic cores. When the content of polysilazane is higher than 5%, the small particles promote sintering and lead to larger shrinkage, and at the same time, the porosity decreases gradually.

Figure 10 shows the flexural strength of ceramic cores with different polysilazane contents at 25 °C and 1,500 °C. With the increase of polysilazane content, both the flexural strength at 25 °C and 1,500 °C firstly increase and then decrease. When the content of polysilazane is 8%, the flexural strength reaches its peak of 33.8 MPa at 25 °C. When the content of polysilazane is 5%, the flexural strength reaches its peak of 13.1 MPa at 1,500 °C. As mentioned above, with the increase of polysilazane content from 3% to 5%, the fracture mode of the ceramic core changes from an intergranular fracture mode to a mixed fracture mode. This change of fracture mode improves the strength of the ceramic cores. However, when the addition of polysilazane continues to increase, the SiO_2 generated by the pyrolysis of the polysilazane is excessive. Due to the softening of SiO_2 during the sintering process, the bonding strength between the matrix particles is weakened, and the mechanical properties of the ceramic cores are worsen. Compared to the flexural strength at 25 °C, this effect is more obvious at 1,500 °C. Therefore, when the content of polysilazane exceeds 8%, the flexural strength at high temperatures tends to decrease.

In conclusion, in order to ensure the ceramic cores have qualified flexural strength and porosity, the optimal amount of polysilazane is 5%. In this case, the flexural strength of the ceramic cores is 31.5 MPa at 25 °C, 13.1 MPa at 1,500 °C, and the porosity is 36.7%.

4.3 Strengthening mechanism

Figure 11 shows the mechanism by which polysilazane enhances the strength of the ceramic cores. According to

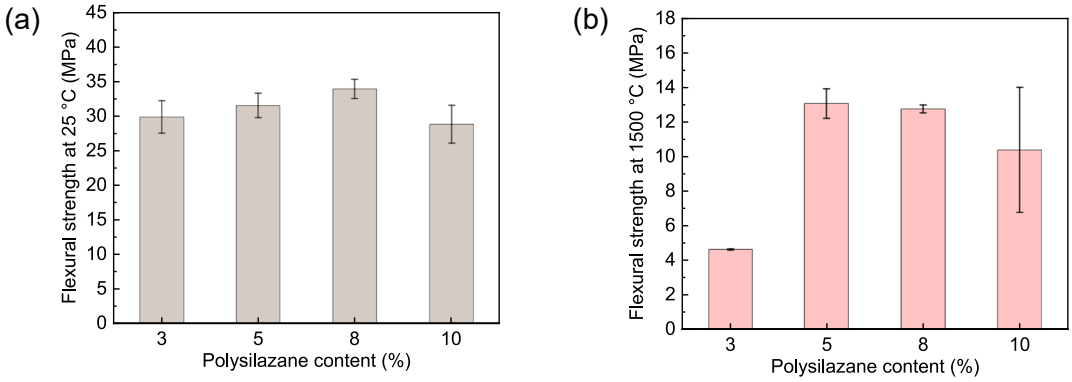

Fig. 10: Effect of polysilazane content on flexural strength of ceramic samples: (a) 25 °C; (b) 1, 500 °C

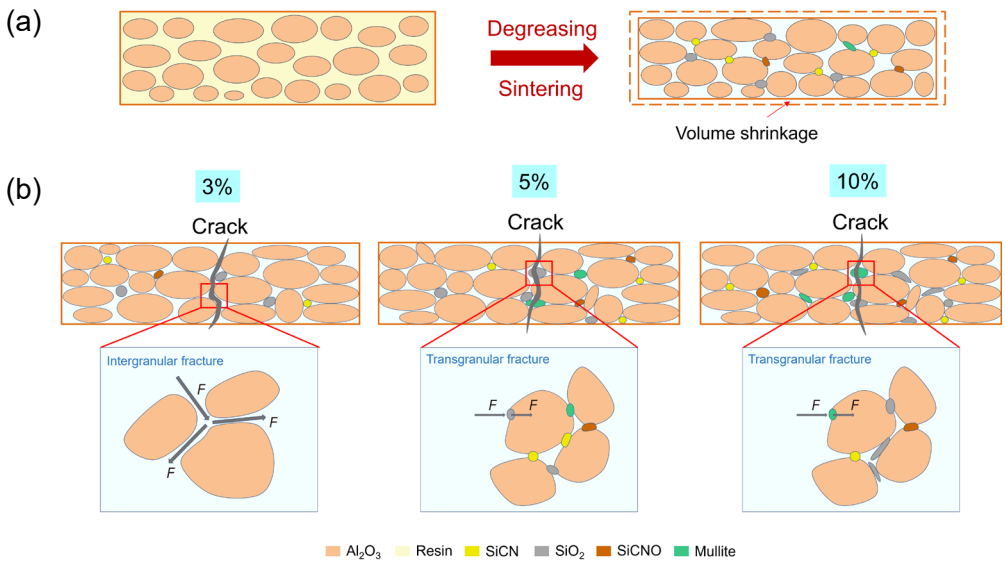

Fig. 11: Strengthening mechanism of polysilazane on ceramic core: (a) structural diagram of ceramic samples before and after sintering; (b) schematic diagram of fracture mode of sintered ceramic samples with different polysilazane contents

previous studies[41,42], polysilazane can be pyrolyzed to produce SiCN, SiO_2, and SiCNO at high temperatures, which is consistent with the results in Figs. 6 and 7 of this study. The pyrolysis products of polysilazane adhere to the surface of ceramic matrix particles in the amorphous phase. Additionally, some of the SiO_2 in the product reacts with Al_2O_3 to form mullite. When the content of polysilazane is 3%, it is difficult to improve the performance of the ceramic core due to the low amount of pyrolysis products. Therefore, when the crack propagates to the surface of the ceramic particles, the crack would propagate along the surface of the ceramic particles because of the low bonding strength between the ceramic particles. With the increase of polysilazane content from 3% to 5%, the small particles produced by pyrolysis fill the pores and connect the ceramic particles, and thus the bonding strength between the particles is enhanced. The fracture mode of the ceramic core changes from intergranular fracture to mixed fracture. The pyrolysis products of polysilazane play an important role in improving the performance of ceramic cores. There are two main reasons[43, 44]: (1) The SiCN in the product has excellent thermal and mechanical properties, and remains thermally stable up to 1,500 ºC; (2) The pyrolysis products adhere to the surface of the ceramic particles in the amorphous phase, improving the bonding strength between the matrix particles. As shown in the local magnification diagram of Fig. 11(b), the strong bonding force between these amorphous phases and the ceramic matrix particles made the crack propagation direction move to the interior of the matrix grains. When the content of polysilazane reaches 10%, the amount of SiO_2 produced by pyrolysis of the polysilazane is excessive. Because SiO_2 is easy to soften at high temperatures, the bonding strength between matrix particles encapsulated by SiO_2 decreases, which leads to the deterioration of ceramic core properties. In summary, when the content of polysilazane is 5%, the ceramic core exhibits excellent mechanical properties.

5 Conclusions

In this study, high performance ceramic cores reinforced with polysilazane were prepared using 3D printing technology. The underlying regulation mechanism of polysilazane on the microstructure and mechanical properties of Al_2O_3-based ceramic core was studied. The main conclusions are as follows:

(1) With the increase of polysilazane content, both the flexural strength and porosity of the ceramic cores firstly increase and then decrease. However, the shrinkage shows an opposite trend. When the content of polysilazane is 5%, the ceramic core exhibits the most excellent comprehensive properties: the flexural strength is 31.5 MPa at 25 °C and 13.1 MPa at 1,500 °C, and the open porosity is 36.7%.

(2) The decomposition products of polysilazane mainly include SiCN, SiCNO, and SiO_2. SiO_2 reacts with the matrix particles to produce mullite. The adhesion of the pyrolysis products to the surface of the ceramic particles improves the properties of ceramic cores. However, when polysilazane is excessive, the softening of SiO_2 at high temperatures leads to the decrease of bonding strength between the ceramic particles.

(3) The fracture mode of ceramic cores changes from intergranular fracture to transgranular fracture with an increase in polysilazane content, thereby enhancing the strength of the ceramic cores. This study provides a new strategy for the preparation of high performance ceramic cores.

Acknowledgments

This work was supported by the National Natural Science Foundation of China (Nos. 52402094, U234120139, and U22A20129); National Defense Basic Scientific Research Program of China (No. JCKY2022130C005); China Postdoctoral Science Foundation (No. 2023M743571); Postdoctoral Fellowship Program of CPSF (No. GZC20232743);

Innovation Project of IMR (No. 2024-PY11); Open Research Fund of National Key Laboratory of Advanced Casting Technologies (No. CAT2023-006); Graduate Education Quality Engineering Project of Anhui Province (No. 2023cxcysj015); Science and Technology Plan Project of Liaoning Province (No. 2024JH2/101900011); National Key Research and Development Program of China (Nos. 2024YFB3714500 and 2018YFB1106600); and the China United Gas Turbine Technology Co., Ltd. (No. J790).

Conflict of interest

The authors declare that they have no known competing financial interests or personal relationships that could have appeared to influence the work reported in this paper.

References

[1] Li X, Niu S X, Wang D S, et al. Microstructure and crystallization kinetics of silica-based ceramic cores with enhanced high-temperature property. Materials, 2023, 16: 606.
[2] Kanyo J E, Schafföner S, Uwanyuze R S, et al. An overview of ceramic molds for investment casting of nickel superalloys. Journal of the European Ceramic Society, 2020, 40: 4955–4973.
[3] Pattnaik S, Karunakar D B, Jha P K. Developments in investment casting process – A review. Journal of Materials Processing Technology, 2012, 212: 2332–2348.
[4] Ke R, Dong Y S. Preparation and properties of water-soluble ceramic core for light alloy investment casting. Materials Today Communications, 2021, 26: 101918.
[5] Liu F C, Fan Z T, Liu X W, et al. Aqueous gel casting of water-soluble calcia-based ceramic core for investment casting using epoxy resin as a binder. The International Journal of Advanced Manufacturing Technology, 2016, 86: 1235–1242.
[6] Zheng W, Wu J M, Chen S, et al. Improved mechanical properties of SiB6 reinforced silica-based ceramic cores fabricated by 3D stereolithography printing. Ceramics International, 2022, 48: 21110–21117.
[7] Shi Y S, Zhang J L, Wen S F, et al. Additive manufacturing and foundry innovation. China Foundry, 2021, 18(4): 286–295.
[8] Zhou H R, Yang H, Li H Q, et al. Advancements in machine learning for material design and process optimization in the field of additive manufacturing. China Foundry, 2024, 21(2): 101–115.
[9] Lu Z L, Cao J W, Song Z Q, et al. Research progress of ceramic matrix composite parts based on additive manufacturing technology. Virtual and Physical Prototyping, 2019, 14: 333–348.
[10] Chen A N, Li M, Xu J, et al. High-porosity mullite ceramic foams prepared by selective laser sintering using fly ash hollow spheres as raw materials. Journal of the European Ceramic Society, 2018, 38: 4553–4559.
[11] Huo M D, Li Q L, Liu J Q, et al. In-situ synthesis of high-performance Al_2O_3-based ceramic cores reinforced with core-shell structures. Ceramics International, 2022, 48: 33693–33703.
[12] Li H, Liu Y S, Liu Y S, et al. Influence of sintering temperature on microstructure and mechanical properties of Al_2O_3 ceramic via 3D stereolithography. Acta Metallurgica Sinica (English Letters), 2020, 33: 204–214.
[13] Li Q L, An X L, Liang J J, et al. Balancing flexural strength and porosity in DLP-3D printing Al_2O_3 cores for hollow turbine blades. Journal of Materials Science & Technology, 2022, 104: 19–32.
[14] Li X, Su H J, Dong D, et al. New approach to preparing near zero shrinkage alumina ceramic cores with excellent properties by vat photopolymerization. Journal of Materials Science & Technology, 2024, 193: 61–72.
[15] Li X, Su H J, Dong D, et al. In-situ $Y_3Al_5O_{12}$ enhances comprehensive properties of alumina-based ceramic cores by vat photopolymerization 3D printing. Additive Manufacturing, 2023, 73: 103645.
[16] Li H, Liu Y S, Liu Y S, et al. 3D printed ceramic slurries with improved solid content through optimization of alumina powder and coupling agent. Journal of Manufacturing Processes, 2021, 64: 1206–1213.
[17] Zhang K Q, Xie C, Wang G, et al. High solid loading, low viscosity photosensitive Al_2O_3 slurry for stereolithography based additive manufacturing. Ceramics International, 2019, 45: 203–208.
[18] Chen H D, Chen B, Li J, et al. Optimization of vat-polymerization binder formulation for 3D printing ceramic slurry using D-optimal mixture experimental design. Composites, Part B: Engineering, 2023, 260: 110777.
[19] Zhang X, Zhang J D, Tian Y H, et al. Photosensitive Al_2O_3 slurry with high solid content and low viscosity. Journal of the Korean Ceramic Society, 2023, 60: 581–590.
[20] Gu Q C, Sun L, Ji X Y, et al. High-performance and high-precision Al_2O_3 architectures enabled by high-solid-loading, graphene-containing slurries for top-down DLP 3D printing. Journal of the European Ceramic Society, 2023, 43: 130–142.
[21] Wang R F, Zhang D M, Zhuang O Y, et al. Effect of Y_2O_3 content on the properties of alumina-based ceramic cores. Applied Mechanics and Materials, 2014, 488–489: 145–149.
[22] Li Q L, Meng X T, Zhang X C, et al. Enhanced 3D printed Al_2O_3 core via in-situ mullite. Additive Manufacturing, 2022, 55: 102826.
[23] Li H, Liu Y S, Li W B, et al. Effect of zirconia content and particle size on the properties of 3D-printed alumina-based ceramic cores. Journal of the American Ceramic Society, 2021, 104: 6015–6028.
[24] Liu X F, Guo X L, Shui G Y, et al. Properties of alumina-based ceramic cores. China Foundry, 2021, 18(6): 593–598.
[25] Li H, Liu Y S, Liu Y S, et al. Effect of sintering temperature in argon atmosphere on microstructure and properties of 3D printed alumina ceramic cores. Journal of Advanced Ceramics, 2020, 9: 220–231.
[26] Li H, Liu Y S, Colombo P, et al. The influence of sintering procedure and porosity on the properties of 3D printed alumina ceramic cores. Ceramics International, 2021, 47: 27668–27676.
[27] Li H, Liu Y S, Liu Y S, et al. Microstructure and mechanical properties of 3D printed ceramics with different vinyl acetate contents. Rare Metals, 2021, 40: 3241–3250.
[28] Liu J Q, Li Q L, Huo M D, et al. Microstructure and mechanical properties of 3D-printed nano-silica reinforced alumina cores. Ceramics International, 2022, 48: 30282–30293.
[29] Li X, Su H J, Dong D, et al. Enhanced comprehensive properties of stereolithography 3D printed alumina ceramic cores with high porosities by a powder gradation design. Journal of Materials Science & Technology, 2022, 131: 264–275.
[30] Mu Y H, Chen J W, An X L, et al. Effect of synergism of solid loading and sintering temperature on microstructural evolution and mechanical properties of 60 vol% high solid loading ceramic core obtained through stereolithography 3D printing. Journal of the European Ceramic Society, 2023, 43: 661–675.

[31] Mitteramskogler G, Gmeiner R, Felzmann R, et al. Light curing strategies for lithography-based additive manufacturing of customized ceramics. Additive Manufacturing, 2014, 1–4: 110–118.
[32] Schmidt J, Altun A A, Schwentenwein M, et al. Complex mullite structures fabricated via digital light processing of a preceramic polysiloxane with active alumina fillers. Journal of the European Ceramic Society, 2019, 39: 1336–1343.
[33] Dong W J, Li Q L, Chen T C, et al. Effect of sintering temperature on microstructure and properties of 3D printing polysilazane reinforced Al_2O_3 core. China Foundry, 2023, 20(5): 387–394.
[34] He C, Liu X E, Ma C, et al. Digital light processing fabrication of mullite component derived from preceramic precusor using photosensitive hydroxysiloxane as the matrix and alumina nanoparticles as the filler. Journal of the European Ceramic Society, 2021, 41: 5570–5577.
[35] Konegger T, Potzmann R, Puchberger M, et al. Matrix-filler interactions in polysilazane-derived ceramics with Al_2O_3 and ZrO_2 fillers. Journal of the European Ceramic Society, 2011, 31: 3021–3031.
[36] Hu L H, Wang Y K, Wang S C, Polymer derived gel-like preceramic precursor of core-shell silicon oxycarbide ceramic for robocasting. Ceramics International, 2019, 45: 23475–23481.
[37] Xiao J, Jia Y, Liu D Q, et al. Three-dimensional printing of SiCN ceramic matrix composites from preceramic polysilazane by digital light processing. Ceramics International, 2020, 46: 25802–25807.
[38] Meng X Y, Yang W X, Deng X. Research on 3D printing process and properties of diamond – resin composites based on digital light processing. Diamond and Related Materials, 2021, 120: 108715.
[39] Shah D M, Morris J, Plaisted T A, et al. Highly filled resins for DLP-based printing of low density, high modulus materials. Additive Manufacturing, 2021, 37: 101736.
[40] Huang M Z, Wu Y Y, Ou J, et al. 3D-printing of polymer-derived SiCN ceramic matrix composites by digital light processing. Journal of the European Ceramic Society, 2022, 42: 5476–5483.
[41] Liu Y, Lin X, Gong H Y, et al. Electromagnetic properties and microwave absorption performances of nickel-doped SiCN ceramics pyrolyzed at different temperatures. Journal of Alloys and Compounds, 2019, 771: 356–363.
[42] Xiao J, Liu D Q, Cheng H F, et al. Carbon nanotubes as light absorbers in digital light processing three-dimensional printing of SiCN ceramics from preceramic polysilazane. Ceramics International, 2020, 46: 19393–19400.
[43] Wang H T, Xie Z P, Yang W Y, et al. Fabrication of SiCN MEMS by UV lithography of polysilazane. Key Engineering Materials, 2007, 336–338: 1477–1480.
[44] Li Q L, Pan Z X, Liang J J, et al. Ceramic composites toughened by vat photopolymerization 3D printing technology. Journal of Materials Science & Technology, 2023, 146: 42–48.